Replicating the Hadley Cell and subtropical jet disconnect in idealized atmospheric models

Molly E. Menzel[1,2], Darryn W. Waugh[2], Zheng Wu[3], and Thomas Reichler[4]

[1]NASA Goddard Institute for Space Studies, New York, New York
[2]Department of Earth and Planetary Sciences, The Johns Hopkins University, Baltimore, Maryland
[3]Institute for Atmospheric and Climate Science, ETH Zurich, Zurich, Switzerland
[4]Department of Atmospheric Sciences, University of Utah, Salt Lake City, Utah

Correspondence: Molly E. Menzel (molly.menzel@nasa.gov)

Abstract. Recent work has shown that variability of the subtropical jet's (STJ) latitude, ϕSTJ is not coupled to that of the Hadley Cell (HC) edge, ϕHC, but the robustness of this disconnect has not been examined in detail. Here, we use meteorological reanalysis, comprehensive climate models, and an idealized atmospheric model to determine the necessary processes for a ϕHC and ϕSTJ disconnect. We find that a decoupling can occur in a dry general circulation model, indicating that large-scale

5   dynamical processes are sufficient to reproduce the metrics' relationship. It is therefore not reliant on explicit variability in the zonal structure, convection, or radiation. Rather, the disconnect requires a sufficiently accurate climatological basic state. Further, we confirm that the robust disconnect between ϕSTJ and ϕHC across the model hierarchy reveals the features' differing sensitivities to midlatitude eddy momentum fluxes; ϕHC is consistently coupled to the latitude of maximum eddy momentum flux but the ϕSTJ is not.

1   Introduction

There is considerable interest in detecting and predicting tropical expansion as a result of increasing greenhouse gases (Seidel et al., 2008; Birner et al., 2014). Early studies examining tropical expansion used various metrics to define the edge of the tropics, including the poleward extent of the Hadley Cell (HC) as well as the subtropical jet's (STJ) location. However, studies presented contradicting conclusions based on their choice of metrics (Seidel et al., 2008; Davis and Rosenlof, 2012; Davis

15   and Birner, 2013; Birner et al., 2014). Subsequent comparisons then exposed there is a disconnect between upper tropospheric and lower tropospheric metrics (Solomon et al., 2016; Waugh et al., 2018). Davis and Birner (2017) similarly categorize them as "zonal circulation" and "meridional circulation" metrics, respectively. One specific result revealed there is no interannual correlation between the STJ latitude and HC edge in reanalyses products or coupled model output (Davis and Birner, 2017; Menzel et al., 2019).

20   Historically, large-scale atmospheric circulation in the lower latitudes has been described by axisymmetric theory. In particular, it is dominated by a thermally direct meridional circulation known as the HC (Lorenz, 1967) where the flow is angular momentum conserving and the circulation's poleward extent is determined by energetic constraints (Held and Hou, 1980; Lindzen and Hou, 1988). Additionally, the STJ is attributed to the HC's poleward advection of angular momentum. As the

HC's upper branch circulates poleward, the zonal-mean zonal wind must increase to maintain angular momentum conservation
and accommodate the flow's decrease in distance to the earth's axis of rotation. This has led to a persistent assumption that the
STJ is co-located and co-varies with the edge of the HC.

Although useful to conceptualize zonal-mean flow, axisymmetric theory is limited as the presence of eddies at higher latitudes resulting from non-axisymmetric processes proves a strong influence on HC dynamics (Schneider, 2006). Rather than
invoking energetic constraints, the HC's meridional extent is instead determined by baroclinic instabilities (Held, 2000) and
can be described by a critical latitude whereby the angular momentum conserving flow can no longer remain stable (Walker
and Schneider, 2006). In this vein, HC edge variability is directly related to that of static stability and midlatitude eddies (Davis
et al., 2016). Indeed, the HC edge's transient response to atmospheric CO_2 follows that of the latitude of maximum eddy momentum flux (Chemke and Polvani, 2019), and is strongly correlated with the eddy-driven jet (EDJ) both interannually and in
response to CO_2 (Kang and Polvani, 2011; Solomon et al., 2016; Davis and Birner, 2017; Staten and Reichler, 2014).

The STJ's relationship with both the HC and midlatitude eddies remains less clear. Despite the logical expectation that
the STJ is strongly coupled to the HC edge, there is no empirical evidence to support it (Waugh et al., 2018; Maher et al.,
2020). The HC edge is not correlated with the latitude of the STJ and it's relationship with the STJ strength is inconsistent.
Interannually, an expanded HC is associated with a weaker STJ but in response to increased CO_2, the HC edge shifts poleward
and the STJ strengthens (Menzel et al., 2019). Further, the two features' have differing transient responses to forcing (Chemke
and Polvani, 2019; Menzel et al., 2019). Is the disconnect between the STJ and HC edge the result of their differing sensitivities
to the midlatitude eddies?

In this study, we use idealized atmospheric modelling to address this question. Specifically, we consider the most idealized
three-dimensional atmospheric model available, a dry general circulation model, with varying basic states. While there are
some unrealistic features with these models, numerous previous studies have demonstrated that they can provide insight into
the dynamical interaction between the tropical and midlatitude circulation (Eichelberger and Hartmann, 2007; Sun et al., 2013;
McGraw and Barnes, 2016). Each model configuration presented uses a thermal relaxation towards an equilibrium temperature,
but range between a zonally-symmetric equilibrium temperature set by an analytic function, and one that is varying in all
dimensions and derived to reproduce the observed atmosphere. Not only does idealized modelling allow us to isolate the
circulation features' sensitivity to midlatitude eddies, it simultaneously reveals the extent to which a simplified atmosphere
can accurately represent the STJ. If none of the dry model simulations can reliably produce a STJ, this would indicate that its
behavior requires processes not included in the model, such as variability in convective processes or sea surface temperatures.
Alternatively, if the model can produce a reasonably accurate STJ and subsequent disconnect from the HC edge, then the
mechanisms involved do not require these processes.

Details regarding these idealized model configurations, along with other method choices made in this study, are included
in Section 2. We then consider metric relationships evident in coupled model and reanalysis product output in Section 3, and
Section 4 presents results from the varying idealized model configurations. Lastly, the implications and limitations of our study
are found in Section 5.
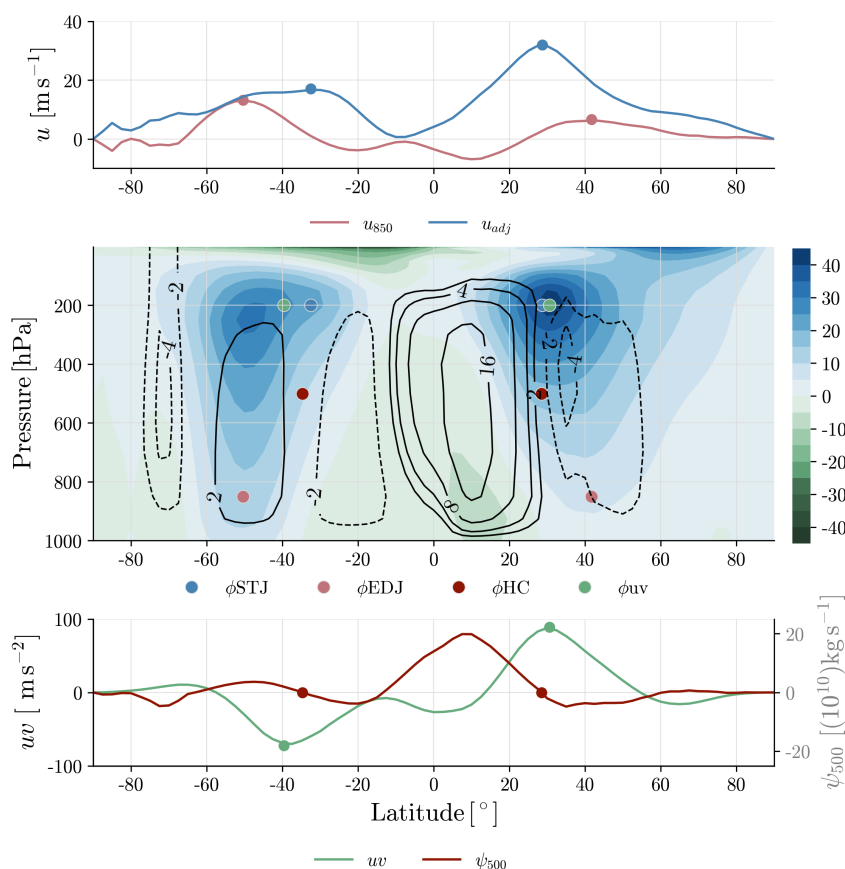
Figure 1. DJF climatology of u_{adj} (top, blue), u_{850} (top, pink), the mean meridional streamfunction (middle, black contour lines, $10^{10}\,\mathrm{kg\,s^{-1}}$), the zonal-mean zonal wind (middle, color contours, $\mathrm{m\,s^{-1}}$), ψ_{500} (bottom, red), and uv (bottom, green) for S-RIP from 1979-2019. Each subplot also shows the metric calculated by its corresponding field, ϕSTJ (top, blue dot), ϕEDJ (top, pink dot), ϕHC (bottom, red dot), ϕuv (bottom, green dot).

2 Models and Methods

2.1 Meteorological Reanalysis Products

60 In this study, we use three reanalyses products provided by the Stratosphere-troposphere Processes And their Role in Climate (SPARC) Reanalysis Intercomparison Project (S-RIP) (Fujiwara et al., 2017) to examine the "observed" atmosphere; the European Centre for Medium-Range Weather Forecast's ERA5 (Hersbach et al., 2020), the second Modern-Era Retrospective analysis for Research and Applications (MERRA-2) (Bosilovich et al., 2016), and the Japanese Meteorological Agency's Japanese 55-year Reanalysis (JRA-55) (Kobayashi et al., 2015). For all fields, we calculate the seasonal average from the zonal-mean monthly output and consider a 42-year time series, 1980-2021. The eddy terms are calculated from 6-hourly output, which

is also available for all included fields. Note, the MERRA-2 output provided by S-RIP has missing values in certain lower-tropospheric levels. Therefore, the MERRA-2 fields with lower levels relevant to metric calculations (i.e. zonal and meridional wind) are taken directly from the National Aeronautics and Space Administration's Global Modelling and Assimilation Office.

2.2 Coupled Climate Model Output

70   In addition to the reanalysis products, we also look at output from coupled climate models that participated in the Climate Model Intercomparison Project, Phase 5 (CMIP5) (Taylor et al., 2012). All analysis is done with the first ensemble member (r1i1p1) of the preindustrial control (piControl) experiment, where the radiative agents of atmospheric composition are held at their pre-industrial levels. We take the zonal-mean monthly output from the same 23 climate models used in Menzel et al. (2019) and present model-mean results. For the eddy calculation, only 4 of those 23 models make available the daily data
75   required for the eddy calculation. Due to this, all CMIP5 analysis pertaining to the eddy fields presents the model-mean across those 4 models.

2.3 Idealized Model Configurations

To diagnose the sensitivity of the HC and STJ to the midlatitude eddies, we perform idealized simulations with a dry atmospheric general circulation model using the Geophysical Fluid Dynamics Laboratory (GFDL) spectral dynamical core in the
80   same configuration as presented in Wu and Reichler (2018). All simulations are forced with a Newtonian relaxation towards one of three different equilibrium temperature profiles.

    The most basic simulation replicates that of McGraw and Barnes (2016), hereafter referred to as "MB16." It's equilibrium temperature, T_{eq} is zonally symmetric and set by the analytic function,

$$T_{eq} = max\{T_{strat}, \left[T_0 - \delta_y sin^2\phi + \varepsilon\chi sin\phi - \delta_z log\left(\frac{p}{p_0}\right)cos^2\phi\right]\left(\frac{p}{p_0}\right)^\kappa\} \qquad (1)$$

85   where $T_{strat} = 200\,\mathrm{K}$ is the stratospheric temperature, $T_0 = 315\,\mathrm{K}$, $\delta_y = 60\,\mathrm{K}$, ϕ is the latitude, $\delta_z = 10\,\mathrm{K}$, p is the pressure, $p_0 = 1000\mathrm{hPa}$ is the reference pressure, and $\kappa = \frac{2}{7}$ is the ratio of gas constant to specific heat of air at constant pressure. This equilibrium temperature deviates from that of Held and Suarez (1994) by it's inclusion of $\varepsilon\chi sin\phi$, which simulates a seasonal profile. ε, set to 20K as in McGraw and Barnes (2016), determines the magnitude of hemispheric asymmetry in the temperature profile while χ modifies that hemispheric asymmetry according to a specific season or month. To simulate the
90   December-January-February season, we choose $\chi = 0.8796$, the mean of χ used in McGraw and Barnes (2016) across those months. Note, the configuration still does not simulate a seasonal cycle. Rather, the seasonal conditions are static in time. In later analysis, we modify δ_z to 15K, 20K, 25K, and 30K to refine this configuration's basic state and test the sensitivity of the circulation features' relationships to this parameter choice.

    To improve the accuracy of the simulated atmosphere in a dry model, Wu and Reichler (2018) present a new equilibrium
95   temperature field that is derived by iteration to reduce the temperature error, as determined by the MERRA-2 (Bosilovich et al., 2016). It's equilibrium temperature is zonally varying and includes seasonality. Since the equilibrium temperature is developed to simulate observed atmospheric temperature, one may infer that it includes implicit impacts of convective and

moist processes. This may be, but the simulation lacks variability of convective and moist processes and only reflects their impacts to setting the basic state. We will refer to this simulation as "WR18."

100   Here, we introduce an intermediate equilibrium temperature profile that, like WR18, is also derived by iteration but designed to provide a zonally symmetric forcing. The appeal of this setup is that it is closer to the simplicity of MB16 while producing similar accuracy to that of WR18. However, simply taking the zonal mean of the WR18 forcing temperature produces a drastically inaccurate atmosphere, with 4 overturning cells in a hemisphere, strong wind jets in the subtropics and polar latitudes, and a corresponding easterly-westerly-easterly-westerly zonal-mean zonal surface wind pattern. Due to this, creation of the

105   zonally symmetric equilibrium temperature file required the same iterative process as that of WR18, reducing the error of the simulated atmosphere according to climatology of MERRA-2. This simulation also allows for seasonality and will be referred to as "WR18z."

All simulations exclude moist and radiative processes, have no topography, and lack any coupling to other climate realms (i.e. ocean, sea ice, land). Note, the equilibrium temperature for WR18 and WR18z were iterated and optimized with topography,

110   but we have set flat conditions in our simulations. Since the dry general circulation model reaches equilibrium quickly, only the first year is excluded in analysis and climatologies are calculated averaging over the remaining 99 years.

2.4   Metrics

For metric calculations, we use the TropD python package (Adam et al., 2018) where applicable. Most metrics are calculated using the seasonal- and zonal-mean fields from monthly output. To calculate the eddy terms in the idealized simulations, we

115   use 6 hourly output and then average the eddy field seasonally and zonally. For all metrics locating a maximum of a field, we apply a quadratic fit to the profile as is done in Menzel et al. (2019). Calculation methods for all metrics can be visualized by Figure 1.

The latitude of the EDJ (ϕEDJ) is found by using TropD_Metric_EDJ to locate the maximum of the the 850 hPa zonal-mean zonal wind, u_{850} (Fig. 1, top, pink). To locate the STJ, we use the "adjusted" method of TropD_Metric_STJ. This method

120   calculates an adjusted wind field, u_{adj}, such that u_{850} is subtracted from the zonal-mean zonal wind vertically averaged between 100-400 hPa (Fig. 1, top, blue). Using the adjusted wind field reduces the signal of the EDJ on the upper tropospheric winds and therefore better distinguishes the STJ from the EDJ. A comprehensive discussion in Adam et al. (2018) states that the adjusted wind method presents a notable difference in the resulting metric and it is more representative of the STJ latitude than by only considering the upper tropospheric wind. Then, rather than simply finding the max of u_{adj}, we define the STJ position

125   (ϕSTJ) as the most equatorward peak of that field. Particularly in the idealized simulations, the adjusted wind may display one weak peak in the subtropics and one strong peak in the midlatitudes. Finding the equatorward peak further mitigates masking by a strong EDJ, enabling proper STJ detection.

We find the HC edge (ϕHC) using the "Psi_500" metric in TropD_Metric_PSI. This method defines ϕHC as the latitude at which the mean meridional streamfunction at 500 hPa, ψ_{500}, crosses zero just north and south of the equator (Fig. 1, bottom,

130   red).
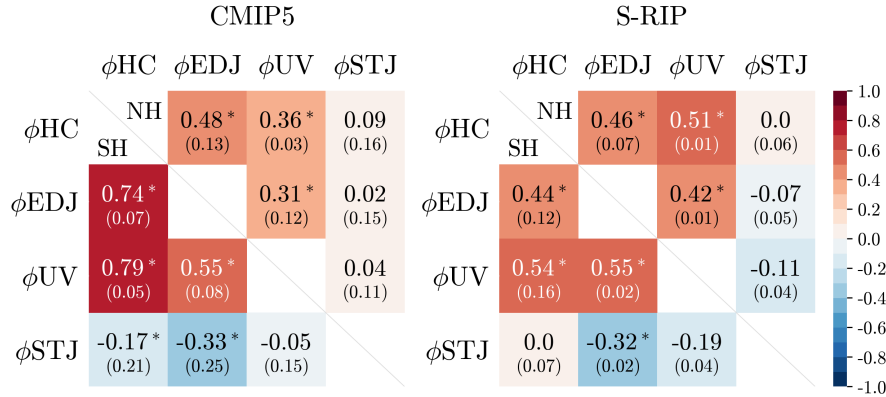
Figure 2. Southern hemispheric (bottom left) and northern hemispheric (top right) interannual correlations for the DJF season of CMIP5 (left) and S-RIP (right). All correlations are the model-mean, the number in parentheses indicates model spread, and the asterisk denotes that correlations are statistically significant.

Following the example of Chemke and Polvani (2019), we also find the latitude of maximum eddy momentum flux (ϕuv) throughout the troposphere, where the eddy momentum flux is defined as $\left[\overline{u^+v^+}\right] cos\phi$ and includes both the transient and stationary eddy terms (i.e. $\left[\overline{u^+v^+}\right] = \left[\overline{u^*v^*}\right] + \left[\overline{u'v'}\right]$ where $[u]$ denotes the zonal mean, $\overline{u}$ denotes the monthly mean, u^* denotes deviations from the zonal mean, and u' denotes deviations from the monthly mean).

135   In calculating correlations between metrics, years are ignored if one of the metrics is not detectable. This is the case if no peak in the adjusted wind profile is equatorward of ϕEDJ. Correlations are defined as significant by a p-value test at a 95% confidence interval (i.e. $P \leq 0.05$).

Lastly, we present a focused view the Northern Hemisphere's (NH) December-January-Februrary (DJF) season. Not only does winter feature a dominant HC compared to summer, spring, and fall, it is also when the STJ is well-separated from the

140   EDJ. This allows for easier detection of both prominent features.

3   Coupled Models and Reanalyses

Before we analyze the idealized model simulations discussed above, we revisit the interannual HC and STJ relationship in meteorological reanalysis products and coupled climate models. As discussed in the introduction, previous work has shown that ϕHC is tied to ϕEDJ (Kang and Polvani, 2011; Davis and Birner, 2017; Staten and Reichler, 2014), but the STJ's behavior

145   is distinct from both (Waugh et al., 2018; Menzel et al., 2019). This is illustrated in Figure 2 for December-January-February (DJF) season. Both the reanalysis products and climate models show a near zero correlation between ϕSTJ and ϕHC for both hemispheres, but ϕHC has a significant positive correlation with ϕEDJ.

We also find low correlations (R < 0.5) between ϕSTJ and ϕEDJ in each hemisphere. Interestingly, there are spurious negative correlations in the SH from frequent masking of the STJ by the EDJ. When ϕEDJ is sufficiently equatorward, the

150   two jets become merged, the midlatitude peak in the adjusted wind profile overshadows the peak in the subtropics, and ϕSTJ
is detected at a more poleward latitude due to it's proximity to ϕEDJ. However, in a more separated state when ϕEDJ is
sufficiently poleward, the adjusted wind profile has a distinct peak in the subtropics, allowing for easy detection of ϕSTJ
at it's more climatological, i.e. equatorward, location. This oscillation between a merged state (ϕEDJ is equatorward, ϕSTJ
detected poleward) and a separated state (ϕEDJ is poleward, ϕSTJ climatologically equatorward), gives rise to a negative
155   correlation. This behavior is also evident when using the default ϕSTJ metric of TropD as in Menzel et al. (2019), where the
ϕSTJ is defined as the location of maximum u_{adj} rather than the most equatorward peak. In that case, the model-mean negative
correlation between ϕSTJ and ϕEDJ is mitigated by more positive correlations of certain models.

      Although the lack of coupling between ϕHC and ϕSTJ has been noted, the physical mechanisms responsible for the disconnect remain unknown. One compelling suggestion, proposed by Davis and Birner (2017), is that the difference is due to the
160   meridional stream function, used to define the HC edge, being physically linked to the distribution of eddy momentum fluxes.

      To see this, first consider the meridional flow balance expressed by Equation 14.7 in Vallis (2017). If we neglect vertical
advection and vertical eddy terms, the equation simplifies to

$$\left(f + \overline{\zeta}\right)\overline{v} = \frac{1}{a cos^2\phi}\frac{\partial}{\partial\phi}\left(\left[\overline{u^+v^+}\right]cos^2\phi\right) \tag{2}$$

where f is the Coriolis parameter, $\overline{\zeta}$ is the zonal-mean relative vorticity, $\overline{v}$ is the zonal-mean meridional wind, a is the radius of
165   the earth, ϕ is the latitude and $\left[\overline{u^+v^+}\right]cos\phi$ is the eddy momentum flux. Close to the equator, eddies are considered negligible
and thus the meridional flow is angular-momentum conserving. However, eddy momentum divergence (the right hand side
of Equation 2) becomes prevalent at higher latitudes. In those regions, the meridional flow is no longer angular momentum
conserving but rather set by those midlatitude eddies.

      In Figure 2, we see that ϕHC positively co-varies with ϕuv with significance in both hemispheres. This supports the sugges-
170   tion that at ϕHC, the meridional flow is in an eddy-dominated regime (Walker and Schneider, 2006; Davis and Birner, 2017;
Chemke and Polvani, 2019).

      On the other hand, variability of the STJ is only related to HC dynamics where the meridional flow is angular momentum
conserving. The result is that while the HC has a direct dynamical relationship to the midlatitude eddies via meridional flow
balance, the STJ does not. This could explain why the correlations between ϕSTJ and ϕuv are less than 0.2.
175   Clearly, there is a distinction between ϕSTJ and those metrics associated with meridional flow balance in an eddy-dominated
regime (i.e. ϕHC, ϕuv, ϕEDJ). At ϕHC, meridional flow is less dependent on angular momentum advection, thus, the expected
coupling between ϕHC and ϕSTJ via angular momentum conservation breaks down.

      Further, the disconnect between ϕHC and ϕSTJ and the link between ϕHC and midlatitude eddies is found in response to
CO_2 forcing. Chemke and Polvani (2019) show that in response to a quadrupling of CO_2, the southern hemispheric (SH) shifts
180   of ϕHC and ϕuv are correlated (R = 0.68 in the annual mean) and have the same rapid transient response to atmospheric CO_2
forcing ($\sim$ 7 years). In response to the same forcing, the STJ shifts poleward minimally and instantaneously while strengthening
with a slower transient response of about 40 years (Menzel et al., 2019).
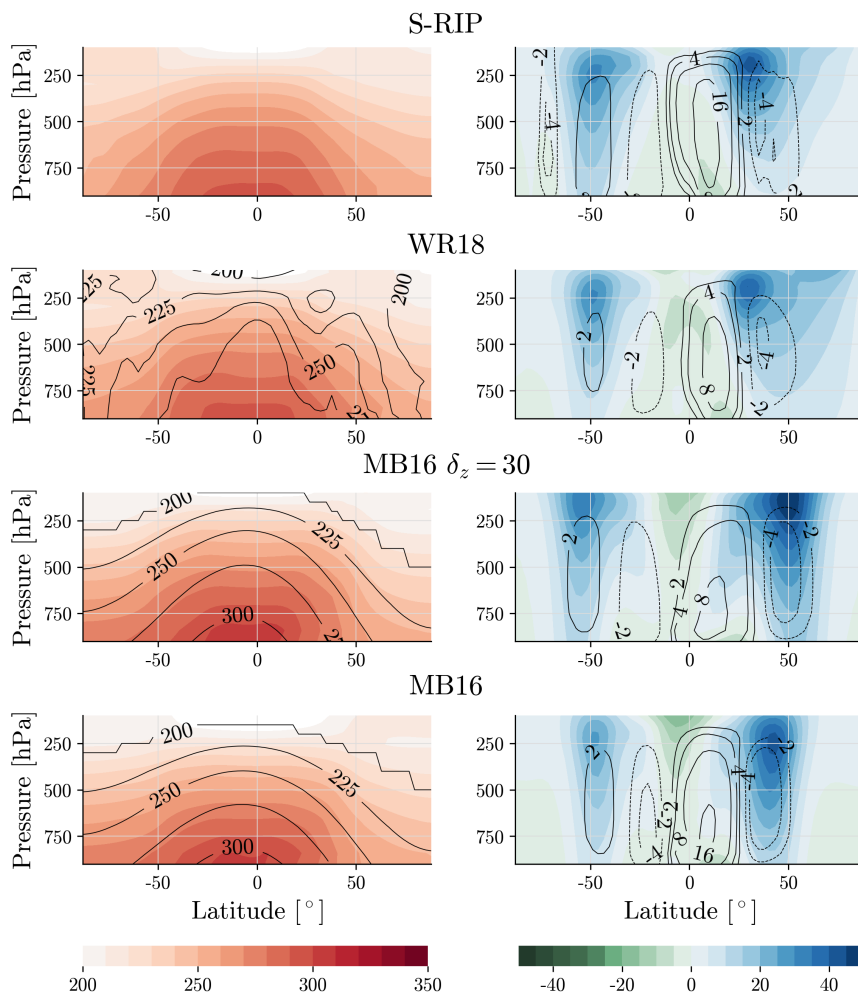
Figure 3. Zonal-mean DJF equilibrium temperature (left, black contour lines, K) and DJF climatology of the simulated temperature (left, color contours, K), zonal wind (right, color contours, $\mathrm{m\,s^{-1}}$), and mean meridional circulation (right, black contour lines, $10^{10}\,\mathrm{kg\,s^{-1}}$) for S-RIP (top), WR18 (middle top), MB16 ($\delta_z = 30$) (middle bottom), and MB16 (default, $\delta_z = 10$) (bottom).

4 Idealized Modelling

The disconnect between the ϕSTJ and ϕHC shown in Section 3 is a robust result across coupled models and reanalysis products. But, it is not known which physical mechanisms are responsible for the result. To identify what model processes are necessary to replicate the ϕSTJ and ϕHC relationship, we start with the most basic idealized atmospheric model, the dry general circulation model presented in MB16, and increase the model's complexity with WR18 and WR18z. Subsequently, we modify the MB16 configuration, improving its simulation of the subtropical circulation.
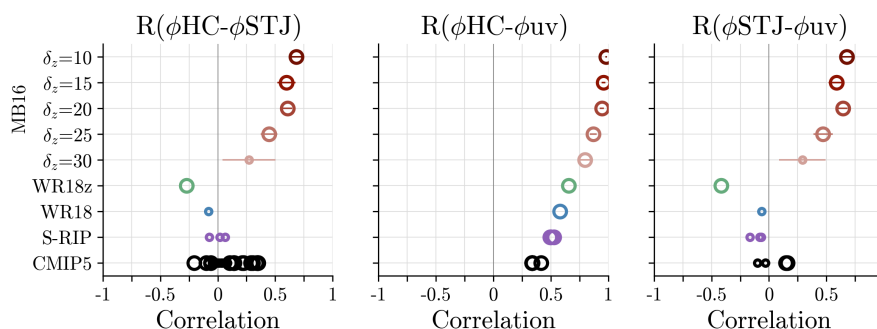
Figure 4. NH DJF interannual correlations between the stated metrics for all model configurations. Here, error bars denote one standard deviation across simulated "seasons" (i.e. MB16 which simulates DJF statically). The larger circles denote correlations found to be significant with 95% confidence ($P \leq 0.05$), and the smaller circles denote insignificant correlations.

4.1 Analytic Equilibrium Temperature

190 We first consider the the most idealized model, MB16. Comparing its climatological basic state with that of S-RIP, figure 3 shows that MB16 produces an atmosphere with the relevant circulation features. The temperature decreases with latitude and altitude (Fig. 3, bottom left), there are distinct Hadley and Ferrel Cells, and the zonal winds increase with height (Fig. 3 bottom right). However, MB16 differs from the S-RIP climatology in notable ways; the zonal winds are barotropic and their maximum is located at the top of the Ferrel Cell rather than on the edge of the HC (Fig. 3, bottom right). Additionally, the meridional

195 streamfunction down not extend as high in the atmosphere as that of S-RIP (e.g. the $8\left(10^{10}\right) \mathrm{kg\,s}^{-1}$ contour line is as high as 200 hPa in S-RIP but only reaches 300 hPa in MB16).

What, then, is the resulting relationship between ϕSTJ and ϕHC in MB16? Figure 4 (red) shows that the MB16 produces a positive correlation between ϕHC and ϕSTJ of about 0.66 Also, ϕHC and ϕSTJ both have a significant positive correlation with ϕuv, indicating that all features are strongly coupled together and set by the midlatitude eddies. Although such a strong

200 correlation between ϕSTJ and ϕHC is in line with simple angular momentum conservation consideration, it is a strong contrast to the reanalysis and coupled model output where their correlations are low (see Fig. 4, black and purple). Therefore, such an idealized atmospheric model as MB16 is unable to replicate the STJ and HC relationship evident in more accurate climatologies.

4.2 Derived Equilibrium Temperature

205 Above we found that there is a coupling between ϕHC and ϕSTJ in an idealized atmospheric model that uses an analytic equilibrium temperature profile, but does it exist in a model with a more realistic atmosphere? The simulated atmosphere of WR18, where the equilibrium temperature is derived iteratively to replicate that from MERRA-2, is shown in Fig. 3. By design, the simulation produces a more accurate atmosphere than MB16. The zonal wind profile shows larger baroclinicity and the distinct maximum in the upper troposphere is co-located with the HC edge (Fig. 3, middle top right). Additionally, the winter

210   HC strength is relatively stronger than that of the summer HC and winter Ferrell Cell when compared to MB16. However, some features remain inconsistent with S-RIP. For instance, it's meridional streamfunction is reduced in strength in the lower latitudes. Additionally, and similar to MB16, the meridional streamfunction does not reach as high in the tropics as in S-RIP. Not shown in this climatology, high latitude zonal winds poleward of $60°$S in WR18 have high variability, impacting features in the midlatitudes.

215   The more accurate atmospheric setup in WR18 produces correlations between ϕHC and ϕSTJ that deviate from strongly positive (Fig. 4, blue) as they are less than 0.1 and insignificant. Meanwhile, ϕHC stays significantly positively correlated with ϕuv, but the correlation between ϕSTJ and ϕuv also reduces to less than 0.1. This result, that ϕSTJ and ϕHC are not positively correlated in WR18, reveals that a disconnect between ϕSTJ and ϕHC is possible in a fully dry atmospheric model. A disconnect is therefore not necessarily dependent on variability in more complex processes, such as convection or radiation.

220   Does it instead depend on zonal asymmetries in the model's forcing? We explore this by considering WR18z, where a new equilibrium temperature field is derived to be zonally symmetric. In the zonal-mean climatology, WR18z produces a similar level of accuracy as WR18 (see Fig. S1 of the Supporting Document). The most apparent differences between the WR18 and WR18z equilibrium temperature are in the lower troposphere at the SH's high latitudes and the NH's midlatitudes, where WR18z appears more variable. Yet, the mean meridional circulation and zonal wind patterns are close to that of WR18. The

225   only subtle differences are that in WR18z compared to WR18, the magnitude of zonal winds in the upper troposphere is larger, and the meridional streamfunction is weaker in the SH summer but stronger in the NH winter.

The resulting correlations between metrics in WR18z are categorically similar to WR18 (see Fig. 4). Although significantly moderately negative, the correlations between ϕSTJ and ϕHC still contrast the strong positive correlations in MB16 and are within the range of correlations from CMIP5. As in WR18 and MB16, ϕHC is positively correlated with ϕuv, but ϕSTJ's

230   correlation with ϕuv is significantly moderately negative. So, a ϕSTJ and ϕHC disconnect is not the result of zonal variability in the model's forcing.

4.3   Modified Analytic Equilibrium Temperature

Given that a decoupling between ϕSTJ and ϕHC is not the result of variability in moist or radiative processes, nor is it the result of zonal variability in the model's forcing, is it possible to replicate the disconnect in a MB16 configuration by improving its

235   basic state?

We explore this by varying δ_z in Equation 1 from it's default value of $10\,\mathrm{K}$ to $15\,\mathrm{K}$, $20\,\mathrm{K}$, $25\,\mathrm{K}$, and $30\,\mathrm{K}$. Physically, increasing this parameter decreases the static stability of the atmosphere, as seen by the lifting of the equilibrium temperature contours in Figure 3 (see the middle bottom left plot). Figure 3 also shows the impact a larger δ_z has on the basic state. The increase in temperature at lower latitudes relative to higher latitudes increases the meridional temperature gradient. This, via

240   thermal wind balance, increases the zonal winds aloft and gives hints of larger baroclinicity in the subtropics. Interestingly, the tropical meridional circulation is weaker in strength compared to that of MB16.

A more specific visualization of the static stability, $\partial\theta/\partial p$, across most model configurations can be seen in the top plot of Figure 5. Most noticeably, WR18 and WR18z have comparable $\partial\theta/\partial p$ as S-RIP in the tropics, just less than $0.1\,\mathrm{K\,Pa}^{-1}$, while
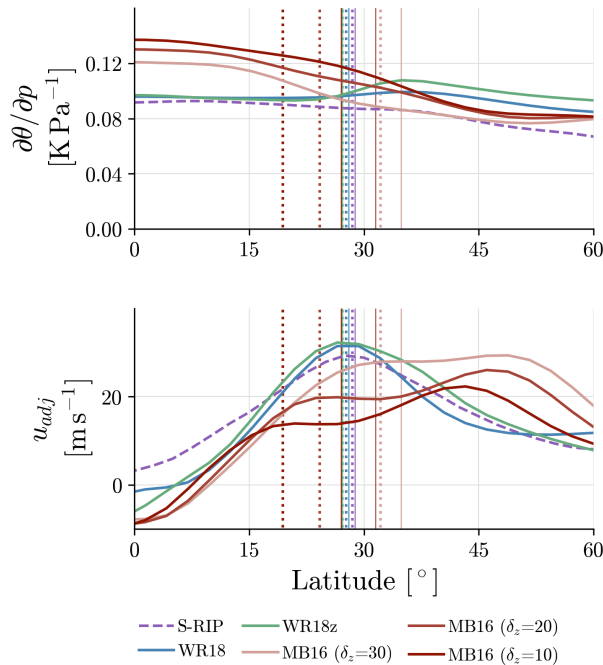
Figure 5. Vertically averaged subtropical static stability (top) and adjusted wind profile (bottom) for S-RIP, WR18, WR18z, MB16 (default, $\delta_z = 10$), MB16 ($\delta_z = 20$), and MB16 ($\delta_z = 30$). The dotted and solid thin lines show the climatological ϕSTJ and climatological ϕHC, respectively, for each corresponding simulation.

all MB16 models simulate $\partial\theta/\partial p \geq 0.12$. In the subtropics, around 30°N, $\partial\theta/\partial p$ in MB16 ($\delta_z = 30$) reduces to a similar value
245 of WR18, WR18z, and S-RIP. Just poleward of 30°N, all model configurations produce $\partial\theta/\partial p$ within a range of 0.08 and 0.11.

Similarly, the bottom plot of Figure 5 compares the profiles of u_{adj} over the same model configurations as in Figure 5. Perhaps unsurprisingly, the more realistic configurations, WR18 and WR18z, are better matches of the u_{adj} profile seen in S-RIP. There is a distinct peak in the subtropics, and u_{adj} non-monotonically decreases until reaching about 45°N. In contrast, the three MB16 configurations shown all reveal a larger peak of u_{adj} in the midlatitudes relative to the subtropics. With a larger
250 δ_z parameter, the strength of u_{adj} in the subtropics increases to a similar magnitude as found in S-RIP, but never to the point of being the dominant peak.

Even so, these changes to the basic state are enough to impact the relationship between ϕSTJ and ϕHC (see Fig. 4). As δ_z increases to 30 K, the significant positive correlation between ϕSTJ and ϕHC reduces to become insignificant and low (~ 0.25). This is within the range of ϕSTJ and ϕHC correlations found in the CMIP5 models. Similarly, the correlation between ϕSTJ
255 and ϕuv reduces to about 0.25 and becomes insignificant as well. All the while, ϕHC remains positively, significantly correlated with ϕuv.

To summarize, the relationship between ϕHC and ϕSTJ as shown by coupled model and reanalysis products can be replicated in a fully dry atmospheric model without variability in moist and radiative processes or zonal structure of the forcing. This is supported by the lack of strong positive and significant correlations between ϕSTJ and ϕHC in the WR18, WR18z, and MB16

260 ($\delta_z = 30$) configurations. The degradation of the significant positive correlations found in the default MB16 configuration occurs as the basic state improves such that a true STJ emerges in the zonal wind profile. Meanwhile, ϕHC's strong and significant correlation with ϕuv is consistent across the entire model hierarchy and ϕSTJ's correlations with ϕuv mirror those correlations between ϕSTJ and ϕHC for each configuration.

5   Concluding Remarks

265 Altogether, we show that a disconnect between the STJ latitude (ϕSTJ) and HC edge (ϕHC) is robust across a hierarchy of models and does not require simulated variability in convective or radiative processes, or a zonally asymmetric basic state. The simulations that oppose this result present such weak zonal winds in the subtropics that the detected STJ is uncharacteristic of its climatological behavior. This is the case for the MB16 configurations with larger values for tropical static stability. As the basic state improves, in the case of the MB16 configurations with decreased static stability in the tropics, a representative STJ

270 emerges and its disconnect from the HC edge and midlatitude eddies remains consistent with increasing model complexity.

This analysis further reveals that the robust nature of a ϕSTJ and ϕHC disconnect is the result of differing sensitivities to the midlatitude eddies. For all levels of complexity, ϕHC remains significantly and strongly correlated to the latitude of maximum eddy momentum flux (ϕuv). The coupling of ϕHC and ϕuv reflects theory that describes the HC's poleward extent as determined by baroclinic instabilities (Held, 2000; Schneider, 2006) rather than energetic constraints (Held and Hou, 1980).

275 In contrast, the STJ is less sensitive to the midlatitude eddies, as evident in the reduced correlations between ϕSTJ and ϕuv given more accurate atmospheric simulations. This is not to say the STJ is entirely unrelated to the midlatitude eddies, rather that their connection is not strong in the zonal-mean, climatological DJF season. Our results leave room for a dynamical relationship between the two features for given regions, or during certain modes of climate variability. An extension of this work to consider those aspects would provide a more detailed view of interaction between the STJ and midlatitude eddies.

280 One major implication is that the robust disconnect between ϕSTJ and ϕHC cautions against conflation of the two metrics. For instance, ϕSTJ should not be used for detection of tropical expansion if a study's interest is in regional impacts (Waugh et al., 2018). Likewise, ϕHC cannot inform behavior of the upper tropospheric subtropical zonal winds that connect to the stratosphere's Brewer-Dobson Circulation (Shepherd and McLandress, 2011).

At the same time, we do not imply that there is no connection between the STJ and HC. Indeed, the STJ's strengthening in

285 response to CO_2 demonstrates the same seasonal, hemispheric, and transient patterns as that of the HC's upper tropospheric upwelling strength and width (Menzel et al., 2023). Rather, the relationship between the STJ and HC is nuanced and level-dependent.

Lastly, our results support use of an idealized dry general circulation model to study large-scale atmospheric dynamics at lower latitudes. So long as care is taken in parameter choices to simulate a sufficiently accurate basic state, inclusion of

290 variability in moist and radiative processes may not be necessary. Such methodological choices are dependent on the research question of interest.

Code and data availability. The output from all idealized model simulations are publicly available via Zenodo (exact link will be provided before final publication). The version of the GFDL dry dynamical general circulation model used in this study, along with the equilibrium temperature in the WR18 configuration, can be found at https://github.com/ZhengWinnieWu/WR_simpleGCM. All coupled model and re-
295 analysis output is freely available; CMIP5 output can be found through the Earth System Grid Federation at https://esgf-node.llnl.gov, refer to https://s-rip.github.io/ for S-RIP.

Author contributions. This study was conceptualized and designed by MEM and DWW. MEM performed the idealized model simulations, conducted the analysis, and created all figures, with input from DWW. ZW provided input files for certain idealized simulations in collaboration with TR. MEM wrote the initial draft with feedback from all co-authors.

300 *Competing interests.* The authors declare no competing interests.

Acknowledgements. Molly E. Menzel is supported by an appointment to the NASA Postdoctoral Program at the Goddard Institute for Space Studies, administered by Oak Ridge Associated Universities under contract with NASA. She also acknowledges support from the NASA Modeling, Analysis, and Prediction program. Molly E. Menzel and Darryn W. Waugh both acknowledge support by the U.S. National Science Foundation (NSF) award AGS-1902409.

References

Adam, O., Grise, K. M., Staten, P., Simpson, I. R., Davis, S. M., Davis, N. A., Waugh, D. W., Birner, T., and Ming, A.: The TropD software package (v1): standardized methods for calculating tropical-width diagnostics, Geoscientific Model Development, 11, 4339–4357, 2018.

Birner, T., Davis, S., and Seidel, D.: Earth's tropical belt, Phys. Today, 67, 38–44, 2014.

Bosilovich, M., Lucchesi, R., and Suarez, M.: MERRA-2: File Specification. GMAO Office Note No. 9(Version 1.1), 73 pp, Global Modeling and Assimilation Office, NASA Goddard Space Flight Center Greenbelt, 2016.

Chemke, R. and Polvani, L. M.: Exploiting the Abrupt $4\times$ CO2 Scenario to Elucidate Tropical Expansion Mechanisms, Journal of Climate, 32, 859–875, 2019.

Davis, N. and Birner, T.: On the discrepancies in tropical belt expansion between reanalyses and climate models and among tropical belt width metrics, Journal of Climate, 30, 1211–1231, 2017.

Davis, N. A. and Birner, T.: Seasonal to multidecadal variability of the width of the tropical belt, Journal of Geophysical Research: Atmospheres, 118, 7773–7787, 2013.

Davis, N. A., Seidel, D. J., Birner, T., Davis, S. M., and Tilmes, S.: Changes in the width of the tropical belt due to simple radiative forcing changes in the GeoMIP simulations, Atmospheric Chemistry and Physics, 16, 10 083–10 095, 2016.

Davis, S. M. and Rosenlof, K. H.: A multidiagnostic intercomparison of tropical-width time series using reanalyses and satellite observations, Journal of Climate, 25, 1061–1078, 2012.

Eichelberger, S. J. and Hartmann, D. L.: Zonal jet structure and the leading mode of variability, Journal of Climate, 20, 5149–5163, 2007.

Fujiwara, M., Wright, J. S., Manney, G. L., Gray, L. J., Anstey, J., Birner, T., Davis, S., Gerber, E. P., Harvey, V. L., Hegglin, M. I., et al.: Introduction to the SPARC Reanalysis Intercomparison Project (S-RIP) and overview of the reanalysis systems, Atmospheric Chemistry and Physics, 17, 1417–1452, 2017.

Held, I. M.: The General Circulation of the Atmosphere, Geophysical Fluid Dynamics Program,Wood's Hole Oceanographic Institution, Woods Hole, MA, pp. 1–70, 2000.

Held, I. M. and Hou, A. Y.: Nonlinear axially symmetric circulations in a nearly inviscid atmosphere, Journal of the Atmospheric Sciences, 37, 515–533, 1980.

Held, I. M. and Suarez, M. J.: A proposal for the intercomparison of the dynamical cores of atmospheric general circulation models, Bulletin of the american Meteorological society, 75, 1825–1830, 1994.

Hersbach, H., Bell, B., Berrisford, P., Hirahara, S., Horányi, A., Muñoz-Sabater, J., Nicolas, J., Peubey, C., Radu, R., Schepers, D., et al.: The ERA5 global reanalysis, Quarterly Journal of the Royal Meteorological Society, 146, 1999–2049, 2020.

Kang, S. M. and Polvani, L. M.: The interannual relationship between the latitude of the eddy-driven jet and the edge of the Hadley cell, Journal of Climate, 24, 563–568, 2011.

Kobayashi, S., Ota, Y., Harada, Y., Ebita, A., Moriya, M., Onoda, H., Onogi, K., Kamahori, H., Kobayashi, C., Endo, H., et al.: The JRA-55 reanalysis: General specifications and basic characteristics, Journal of the Meteorological Society of Japan. Ser. II, 93, 5–48, 2015.

Lindzen, R. S. and Hou, A. V.: Hadley circulations for zonally averaged heating centered off the equator, Journal of Atmospheric Sciences, 45, 2416–2427, 1988.

Lorenz, E.: The nature and theory of the general circulation of the atmosphere, World meteorological organization, 161, 1967.

Maher, P., Kelleher, M. E., Sansom, P. G., and Methven, J.: Is the subtropical jet shifting poleward?, Climate Dynamics, 54, 1741–1759, 2020.

McGraw, M. C. and Barnes, E. A.: Seasonal sensitivity of the eddy-driven jet to tropospheric heating in an idealized AGCM, Journal of Climate, 29, 5223–5240, 2016.

Menzel, M. E., Waugh, D., and Grise, K.: Disconnect between Hadley cell and subtropical jet variability and response to increased CO2,
345   Geophysical Research Letters, 46, 7045–7053, 2019.

Menzel, M. E., Waugh, D. W., and Orbe, C.: Connections between Upper Tropospheric and Lower Stratospheric Circulation Responses to Increased CO 2, Journal of Climate, 36, 4101–4112, 2023.

Schneider, T.: The general circulation of the atmosphere, Annu. Rev. Earth Planet. Sci., 34, 655–688, 2006.

Seidel, D. J., Fu, Q., Randel, W. J., and Reichler, T. J.: Widening of the tropical belt in a changing climate, Nature geoscience, 1, 21, 2008.

350 Shepherd, T. G. and McLandress, C.: A robust mechanism for strengthening of the Brewer–Dobson circulation in response to climate change: Critical-layer control of subtropical wave breaking, Journal of the Atmospheric Sciences, 68, 784–797, 2011.

Solomon, A., Polvani, L., Waugh, D., and Davis, S.: Contrasting upper and lower atmospheric metrics of tropical expansion in the Southern Hemisphere, Geophysical Research Letters, 43, 2016.

Staten, P. W. and Reichler, T.: On the ratio between shifts in the eddy-driven jet and the Hadley cell edge, Climate dynamics, 42, 1229–1242,
355   2014.

Sun, L., Chen, G., and Lu, J.: Sensitivities and mechanisms of the zonal mean atmospheric circulation response to tropical warming, Journal of the Atmospheric Sciences, 70, 2487–2504, 2013.

Taylor, K. E., Stouffer, R. J., and Meehl, G. A.: An overview of CMIP5 and the experiment design, Bulletin of the American Meteorological Society, 93, 485–498, 2012.

360 Vallis, G. K.: Atmospheric and oceanic fluid dynamics, Cambridge University Press, 2017.

Walker, C. C. and Schneider, T.: Eddy influences on Hadley circulations: Simulations with an idealized GCM, Journal of the atmospheric sciences, 63, 3333–3350, 2006.

Waugh, D. W., Grise, K. M., Seviour, W. J., Davis, S. M., Davis, N., Adam, O., Son, S.-W., Simpson, I. R., Staten, P. W., Maycock, A. C., et al.: Revisiting the relationship among metrics of tropical expansion, Journal of Climate, 31, 7565–7581, 2018.

365 Wu, Z. and Reichler, T.: Towards a More Earth-Like Circulation in Idealized Models, Journal of Advances in Modeling Earth Systems, 10, 1458–1469, 2018.